High purity hydrogen from biogas via Steam Iron Process: preventing reactor clogging by interspersed coke combustions

By

J. Lachén, J. Herguido and J.A. Peña*

Aragon Institute of Engineering Research (I3A), Universidad Zaragoza;

c/ Mariano Esquillor, 3;

E50018 Zaragoza (SPAIN)

Telephone: +34 976 762 390

Fax: +34 976 762 043

e-mail: jap@unizar.es

*corresponding author

Abstract

Production of high purity hydrogen from biogas by combined dry reforming of methane and steam iron process (SIP), outlines a serious drawback with the possible formation of coke deposits along reduction steps of the iron oxide. Steam used along reoxidations, which regenerates the iron oxide and force the release of high purity hydrogen, could also be responsible of the gasification of such coke deposits and the consequent contamination of hydrogen with carbonaceous species such as CO or CO_2. Oxidations at low enough temperature can inhibit coke gasification, but paradoxically, increasing amounts of coke upon repeated cycles will provoke reactor clogging sooner or later. To circumvent this issue, a strategy consisting of interspersing coke combustion stages with diluted oxygen within the regular cycles of reduction with biogas and reoxidation with steam releasing hydrogen, has been analyzed with three solids based on iron oxide. It has been verified that including coke combustion stages within the regular scheme of redox cycles, not only counteracts both bed clogging and catalyst deactivation by coking, but also breaks down the trend to lose (by sintering) active material for the redox process, thus allowing the extension of the useful life of the solid.

Keywords: biogas, biomass to hydrogen, chemical looping, catalyst, steam-iron process, coking

1. INTRODUCTION

It is well known that the progressive exhaustion of fossil fuels as well as environmental degradation, gave birth in the past seventies to the concept of "*hydrogen economy*" [1,2]. Since its combustion only produces water, the use of hydrogen as energy vector supposes an environmentally friendly alternative that can be used in fuel cells (e.g. PEMFC), to replace the traditional internal combustion engines in service in the mobility sector. In this context however, environmental friendliness strongly depends on the type of resources used to produce hydrogen. Currently, most of it is produced from natural gas and carbon [3], and even if electrolysis of water is proposed as alternative source, it is important noting that nowadays 70 % of the electricity is also produced from fossil fuels [3]. A suitable solution for using fossil fuels in an environmentally sustainable way, is applying carbon (i.e. CO_2) capture and storage technologies, but this last solution results in a significant loss of competitiveness of the hydrogen produced due to its associated costs [4].

Instead of the traditional reforming processes and subsequent purification of hydrogen streams by PSA (*Pressure Swing Adsorption*), in this work it is presented the *Steam-Iron Process* (SIP) as a joint process for producing and purifying hydrogen within the same reactor [5,6]. SIP is directly related with *Chemical Looping Combustion* (CLC) and *Chemical Looping Hydrogen production* or *Reforming* (CLH or CLR) [6–8]. Essentially, SIP consists of carrying out cyclically, two consecutive stages (see Figure 1a): first, the reduction of a metal oxide (typically iron oxides) and second, its subsequent reoxidation with steam, releasing high purity hydrogen, easily separable from unreacted water by condensation. Given the nature of the process, SIP method allows the intensification of the process of production and purification of hydrogen. Iron oxides, either hematite (Fe_2O_3) or magnetite (Fe_3O_4) of synthetic [9,10] or natural origin [11,12], are the most traditionally used oxygen carriers due to their high availability, high oxygen transfer capacity, low toxicity and low costs [13]. The use of iron ores or wastes from the steel industry, implies a much cheaper option compared to those produced in laboratory [14,15], although the presence of natural impurities such as CaO, Al_2O_3, or SiO_2 slows down the

reduction rate compared to that of pure iron oxides [16].

One of the main advantages of SIP for producing and purifying hydrogen is that any stream with sufficient reducing capacity is suitable for being employed as reductant [10,17,18], having previously been tested in our laboratory the use of several alcohols [19,20], as well as mixtures of acids, alcohols and ketonic/aldehydic compounds simulating a desulphurized bio-oil [21] with promising results.

Present work analyzes the use of a synthetic sweetened biogas as raw material to produce hydrogen. It might come from the anaerobic decomposition of organic matter, being methane and carbon dioxide their main components, with a variable proportion of both (CH_4 50-70 v% and CO_2 30-50 v%) in its composition, depending on its origin and treatment [22]. Biogas can be produced from landfills of municipal solid wastes, sewage sludges or agricultural and livestock wastes [23]. Currently, the most common application of this resource is its combustion for production of hot sanitary water fulfilling the needs of the plant, and/or its use for production of electricity by turbines or internal combustion engines [24]. Finally, it opens the possibility of producing "*bio natural gas*" for supply of the existing natural gas network [25].

The use of this kind of raw materials as reducing agent for SIP has been previously tested in our laboratory, forcing it to react with *tailor-made* iron oxides [26,27] and iron ores [12], as well as through the use of cobalt ferrites ($CoFe_2O_4$) [28]. In all cases, it was required the addition of a nickel aluminate catalyst [9] for improving their activity for the methane dry reforming reaction (MDR) (r.1) along reductions of the solid (i.e. reduction stages).

$$CH_4 + CO_2 \rightleftharpoons 2CO + 2H_2 \qquad \text{(r.1)}$$

Due to the cyclic nature of SIP, one of the factors that determines the viability of the process is the ability of the oxygen carrier to keep its activity along an undefined number of redox cycles; or in other words, its ability to resist sintering phenomena. These undesirable behaviour determine the operating temperature along reductions and oxidations [12,28], trying to maximize the production of purified hydrogen while lowering the operation temperature along

reduction stages (ca. 700 ºC).

Given that along reductions the feed is composed of carbonaceous species like CH_4 and CO_2, and that nickel, the catalytically active species, exhibits a high trend to carbon formation when working at low temperatures of reduction (650 ºC – 750 ºC), a progressive accumulation of coke can be foreseen along repeated cycles of redox operation. Graphitic coke, associated to nickel catalyst particles, and amorphous carbon deposits at a minor extent, have been identified by Raman spectroscopy in similar reacting systems as those proposed in this work [9,26,27]. Graphitic coke is known by its reluctancy to be gasified with steam, but can be oxidized in presence of diluted oxygen at moderate temperatures (below 500 ºC) [28]. Presence of coke deposits, severely restricts the temperature allowed in the subsequent oxidation step. In order to prevent its gasification with steam, operating temperatures along oxidations should not be higher than 500 ºC [28]. In this context, avoiding gasification of carbon is crucial, since emerging CO_x species (CO and CO_2) would contaminate the hydrogen produced according to reaction (r.2).

$$C + H_2O \rightarrow CO + H_2 \qquad \text{(r.2)}$$

As can be deduced, if coke produced in reductions is not removed along subsequent oxidations, the reactor will clog sooner or later. Therefore, interspersing of coke combustion stages with air should be mandatory to increase successfully the number of redox cycles, and consequently increase the performance of the whole process. Figure 1b shows a conceptual diagram describing the alternance of redox cycles (composed by reductions with sweetened biogas and oxidations with steam) and oxidations with diluted oxygen to burn out coke and regenerate the iron oxides. Oxidation with diluted air has been performed every four conventional SIP cycles.

2. EXPERIMENTAL

2.1 Oxygen carriers

The oxygen carriers tested in this work have been the following: a) a synthetic iron oxide (Fe_2O_3, 98 wt%) doped with low proportions of alumina (Al_2O_3, 1.75 wt%) and ceria (CeO_2,

0.25 wt%), called "*triple*" oxide across the text [19], b) a lab-made cobalt ferrite with stoichiometric formula $Al_{0.53}Co_{0.8}Fe_{1.6}\ O_4$ [28], and c) an iron ore with high content of hematite (Fe_2O_3, up to 81.3 wt%) and natural impurities (i.e. CaO, Al_2O_3, CO_3Na_2…). Its nominal composition can be consulted in the work of Lachén et al. [12]. This last is commercialized with name "*Superfine*", and was supplied by *PROMINDSA* (Tierga, *Spain*).

Triple oxide was synthesized in laboratory by citrates method [29]. Essentially, it consists of the preparation of a 1M solution from the corresponding nitrate salts of each metal (*Sigma Aldrich* 99.5 wt%). Once the aqueous solution is prepared, a 1.1 M solution of citric acid is added under stirring at 70 °C. Once gel is formed, it was dried overnight and calcined in a double ramp: first up to 350 °C along 2.5 h, and then up to 850 °C along 8 h. Cobalt ferrite was synthesized by joint fusion method [30]: once the corresponding nitrate salts of each of the metals were weighted and mixed, they were calcined for 6 hours at 1000 °C. Finally, in case of iron ore, its only pre-treatment consisted in calcinating at 800 °C for 8 hours to remove carbonates.

2.2 Catalyst

The catalyst selected for this work was a nickel aluminate ($NiAl_2O_4$) with 10 wt% of NiO in excess above its stoichiometric composition. It was optimized in previous works of our research group [9], being synthetized by co-precipitation at increasing pH method [31]. First step consisted of preparing an aluminum nitrate and a nickel nitrate solutions 1M and 0.631 M respectively. Once mixed, an aqueous solution of NH_4OH (30 wt%) was added to the resulting solution with continuous stirring at 45 °C, at pH 7.8-7.9. Finally, it was filtered, washed, and dried overnight at 100 °C, and finally calcined at 900 °C for 3 hours.

All solids described in the above paragraphs, oxygen carriers and catalyst, were ground and sieved to a particle size between 100 and 200 µm.

2.3 Experimental setup

The experimental system consists of a vertical fixed bed reactor built in quartz ($Ø_i$= 0.013 m).

The mass of solids in the bed was 2.5 g. It was composed of 67.5 wt% of oxygen carrier, 7.5 wt% of catalyst and 25 wt% of silicon carbide (previously milled and sieved to 100-200 μm). All solids were mechanically mixed until achieving a homogeneous bed. Silicon carbide was added to prevent possible temperature profiles and avoid the formation of preferential paths of gas along the bed.

Reduction stages were carried out at 700 °C supplying 250 mL(STP)/min composed of 25 v% of an equimolar mixture of CH_4 and CO_2 (simulating a previously desulphurized biogas with low methane content), 5 v% N_2 as internal standard and Ar up to balance. Oxidation stages with steam were carried out at 500 ºC, feeding the same flow than that used along reduction stages. Along oxidations, the feedstock was composed of 25 v% of steam, 5 v% N_2 as internal standard and Ar up to balance. Oxidation stages with steam always lasted 60 minutes.

Finally, the oxidation stages in which diluted oxygen was used (coke combustion stages), were carried out at 600 °C, feeding the same total flow than in previous stages of reduction and oxidation with steam (i.e. 250 mL(STP)/min). In this case though, feed was composed of 3 v% O_2, 5 v% N_2 as internal standard and Ar to balance.

Water supply was performed by an HPLC pump (*Shimadzu LC-20AT*). Advance degree of reactions was measured analyzing the exhausted gases using a μ-GC *Agilent 490* with *Molisieve 5 Å* and *Poraplot Q* columns. Water was always forced to condense at the exit of the reactor with the aid of a *Peltier* module to preserve the integrity of the μ-GC.

3. RESULTS AND DISCUSSION

3.1 Behaviour of oxygen carriers along reduction stage

Figure 2 presents the evolution with time of the molar flows of reaction products along the first reduction stage for each oxygen carrier tested. Even though all three exhibit a similar behavior, it is necessary to distinguish between solids in which the main oxygen-carrier is hematite (*triple* oxide, and iron ore) and the one in which its main component is cobalt ferrite. XRD

diffractograms of the different solids prior to or before reduction and oxidation stages can be consulted in previous works [12,19,32].

Figure 2a shows the evolution of the products for hematite-based carriers. The following steps can be identified: along the first 5 minutes (period A_1), the mixture of CH_4 and CO_2 simulating a sweetened biogas, allows the on-site activation of the catalyst due to the reduction of NiO to metallic Ni by CH_4 (r.3). Emerging metallic Ni catalyzes the methane dry reforming (MDR) reaction (r.1) whose main gaseous products are CO and H_2. In parallel along this period, hematite (Fe_2O_3) is also reduced to magnetite (Fe_3O_4) by the increasing amounts of H_2 and CO following reactions (r.5) and (r.6).

Period A_2 extends between ca. minutes 5 and 23 (represented by slashed vertical lines). Along this period, it takes place the reduction of Fe_3O_4 to metallic Fe (r.7 and r.8). Since it is strongly influenced by the thermodynamic equilibrium between magnetite and metallic iron, the molar flows of exhaust gases along A_2 are almost constant with a low slope towards equilibrium, as it has been described in previous studies [12,19–21,26]. Once the reduction of the solid has finished (i.e. iron oxides have been completely depleted) it begins period B, for which distribution of molar flows agrees with the theoretically predicted (by minimization of Gibbs free energy, ΔG) thermodynamic equilibrium.

$$3NiO + CH_4 \longrightarrow 3Ni + CO + 2H_2O \quad \text{(r.3)}$$

$$3Fe_2O_3 + CH_4 \longrightarrow 2Fe_3O_4 + CO + 2H_2 \quad \text{(r.4)}$$

$$3Fe_2O_3 + CO \rightleftharpoons 2Fe_3O_4 + CO_2 \quad \text{(r.5)}$$

$$3Fe_2O_3 + H_2 \rightleftharpoons 2Fe_3O_4 + H_2O \quad \text{(r.6)}$$

$$Fe_3O_4 + 4H_2 \rightleftharpoons 3Fe + 4H_2O \quad \text{(r.7)}$$

$$Fe_3O_4 + 4CO \rightleftharpoons 3Fe + 4CO_2 \quad \text{(r.8)}$$

On the other hand, Figure 2b shows the evolution of the exhausted gases of the reduction stage for cobalt ferrite used as oxygen carrier. In this case both, activation of the catalyst and reduction of cobalt ferrite to iron and cobalt, occur progressively in a single step (A) [28,33].

Finally, once the oxygen has been depleted from ferrite, the distribution of molar flows of gaseous species agrees well with the theoretical thermodynamic equilibrium (period B). Also, as consequence of thermodynamics, period B in both Figure 2a and 2b, renders similar proportions of gaseous species regardless of the nature of the original oxygen carrier (hematite or ferrite).

3.2 Stability of oxygen carriers along redox (biogas/steam) cycles

Figure 3 shows the evolution of the CO ratio (eq.1) along the reduction stages of the first four cycles (see Figure 1) for iron ore (Figure 3a), triple oxide (Figure 3b) and cobalt ferrite (Figure 3c). This ratio reflects the proportion between reducing (CO) and oxidizing (CO_2) carbonaceous species at the exit of the reactor.

$$CO\ ratio = \frac{CO\ molar\ flow}{CO\ molar\ flow + CO_2\ molar\ flow} \qquad \text{(eq.1)}$$

A similar phenomenon occurs with both oxides. First reduction from fresh solid exhibits a slightly different behaviour from that of the following. The reason is that only along the first reduction it takes place the reduction of hematite to magnetite as described in Figure 2a. Every reduction is followed by an oxidation with steam (reverse r.7) that completes the cycle. The oxidation of the solid up to hematite in the conditions selected for its regeneration (i.e. with steam at 500 ºC and atmospheric pressure) is thermodynamically impeded. The result is that, as the number of cycles increases, the time required to completely reduce the solid becomes lower. This fact is due to a progressive decrement of the reducible mass of solid caused by sintering effects that, upon reoxidation, will turn in a lower mass of accessible oxide along the subsequent reduction stage.

The results obtained for consecutive reducing stages employing cobalt ferrite can be seen in Figure 3c. Comparing the first cycle with the following, it can be noted a decrease in the time required to reduce the solid (i.e. up to achieving a CO ratio governed by equilibrium). However, unlike the results obtained with hematite oxides, the gap between the 2nd, 3rd and 4th cycles with ferrite is practically negligible. The reason for that reduction in the time needed for

achieving the equilibrium when increasing the number of cycles, is not so much due to sintering, but to the low rate of oxidation of this material with steam, and it has to do with the length of the oxidation period (which was kept constant in 60 minutes in the present study): following a reduction stage, in the subsequent oxidation with such low oxidation rate, only a portion of the previously reduced metal is reoxidized.

Figure 4 displays the hydrogen produced (g) per 100 g of solid after every oxidation stage for each oxygen carrier. Figure also shows, for the sake of comparison, the theoretical stoichiometric maxima attainable for each solid, represented as horizontal dot-dashed lines. The greater drops of hydrogen production from one cycle to the next can be seen in the case of *triple* oxide. That can be ascribed to the previously mentioned sintering phenomenon, which is especially significant in this solid.

In case of using iron ore, only a slight decrease is observed from one cycle to the next, as has been described elsewhere [12]. It is probably due to the good properties, in terms of structural stability against thermal sintering, conferred by the impurities present in the iron ore [16]. However, iron ore presents a lower oxidation rate, resulting in a lower production of hydrogen upon reoxidation with steam. It is worth remembering that all oxidation stages with steam lasted 60 minutes independently of the solid or the treatment to compare their performance.

Cobalt ferrite also shows a low oxidation rate, what combined with a fixed length of 60 minutes for the oxidation stage, turns into low H_2 yields (i.e. g H_2 for every 100 g of solid processed). It exhibits similar yields after the first cycle than that with iron ore. However, unlike oxides based in hematite, cobalt ferrite presents a slight gradual increase in the amount of hydrogen produced along the redox cycles. A hypothesis to explain this phenomenon consists in the segregation of the original ferrite into more easily oxidizable species along the consecutive redox cycles. In other words, part of the cobalt, and/or iron previously reduced, might be reoxidized to disaggregated Co_3O_4 or Fe_3O_4, instead of forming the original cobalt ferrite structure again. Segregation problems like the one described have been observed in other mixed oxides such as

perovskites [34] as well as in other spinels [35]. Emerging of these segregated species might explain the higher oxidation rates compared to that of the original cobalt ferrite [36], that consequently could enhance the production of hydrogen along cycles. Of course, this hypothesis should be subjected to the condition that this effect prevails, at least for a given number of cycles, over the loss of activity due to sintering.

In previous studies with these solids [12,26–28,33], it was detected the formation of carbonaceous deposits (coke) along reductions. It was evidenced mainly by a significant atomic unbalance of carbon between feed and exhaust gases. This fact was also corroborated by different characterization techniques such as EDS and Raman [26,27]. According to Raman spectra performed in materials like the ones used here, graphitic carbon seems to be mostly ascribed to nickel catalyst particles. Structured carbon is denoted by the high intensity of G band (1550 cm^{-1}), present in these samples. Other authors have found analogous results in similar reacting systems [37]. Role of different iron oxides respecting coke formation in similar reactive systems (chemical looping dry reforming), have been also described recently by other authors [38]. Nevertheless, despite these deposits, along all cycles performed and regardless of the oxygen carrier used, hydrogen was produced with high purity, being the content of carbonaceous species upon reoxidation with steam, always below 50 ppm. Gasification of the coke deposited on the bed along the previous reduction stages (r.2) was avoided by setting a relatively low temperature of 500 ºC as oxidation temperature [28]. However, following this regeneration strategy, coke was not being removed, and its accumulation caused a progressive increase in the overpressure of the reactor, making unpractical the realization of more than 4 consecutive redox cycles in our fixed bed reactor.

3.3 Effect of interspersing oxygen combustion stages

A possible way to cope with the previously mentioned problem, consisted in including interspersing coke combustion stages with diluted oxygen between redox cycles. Since this task is complex and the amount of coke deposited was not too high, it was decided that oxygen

would be used every 4 redox cycles following the series: reduction with biogas + oxidation with steam up to four times (see Figure 1b). On this way, high purity hydrogen was released in four consecutive cycles; after the fourth, it was included a stage of oxidation with diluted oxygen to burn out the carbon deposited along the four previous reductions. Exhaust gases from combustion were vented.

In Figure 5 it can be observed the amount of hydrogen (g) produced along every oxidation with steam per 100 g of solid. Analyzing first the case of *triple* oxide, it is observed a noticeable increase in the amount of hydrogen produced after the incorporation of each coke combustion stage (marked by vertical dashed lines after 4^{th}, 8^{th} and 12^{th} cycle). This can be mainly attributed to the fact that along these stages, not only coke was removed by combustion but also metallic iron, that was not oxidizable by steam due to thermodynamic limitations, is now reoxidized with oxygen up to the original hematite phase. That causes an increment in the effective amount of reducible material in the subsequent reduction (i.e. 5^{th}, 9^{th} and 13^{th} stages) with biogas, and therefore more iron is susceptible of being re-oxidized by steam releasing hydrogen.

Regarding the effect of combustion stages on iron ore, it exhibits a similar qualitative trend than that of *triple* oxide (Figure 5). From a quantitative standpoint, it even reaches better hydrogen yields per 100 g of solid for cycle 5^{th} and above than in the previous four cycles. However, what it is most remarkable regarding this solid, is that the increment in the activity of the iron ore after introducing the first stage of coke combustion (i.e. after 4^{th} cycle), almost doubles the H_2 yield respecting its previous reduction, being this even considerably greater than the amount of H_2 released after the very first cycle. This phenomenon must be necessarily associated with the fact that this oxide was being only partially reduced in cycles before the combustion stage. After combustion stage, this formerly inert fraction is reduced, increasing therefore, the amount of re-oxidizable solid and thus the hydrogen produced per 100 g of solid.

Cobalt ferrite exhibits, although smooth, the opposite trend than that seen with *triple* oxide and iron ore: the greater the number of cycle, the greater the yield towards H_2 upon reoxidation with

steam. This is certain for the first four cycles. After them, the reoxidation with air produces a slight increment in the amount of H_2 released per 100 g of solid, rendering as the other solids do, greater yields than those found after the first cycle. Along the next cycles (i.e. 5^{th} on), yields keep almost constant stabilized in values of around 1.7-1.8 g H_2/100 g of solid.

Figure 6 shows the evolution of the CO ratio (eq.1) along reductions carried out immediately after the coke combustion stages (5^{th}, 9^{th} and 13^{th}), compared with that of fresh solid (1^{st} reduction) and with that carried out just before the first combustion stage (4^{th} reduction), for all three solids (*triple* oxide -Figure 6a-, iron ore -Figure 6b– and cobalt ferrite -Figure 6c-). For *triple* oxide (Figure 6a), it can be noted how after applying coke combustions, curves of CO ratio present similar shape than that for fresh solid (i.e. they include both A_1 and A_2 stages -see Figure 2a as reference-). This indicates that indeed, and unlike for the curves before combustion (4^{th} reduction in Figure 6a), not only magnetite but also hematite is being reduced (describing stage A_1 as in Figure 2a). Moreover, from a quantitative point of view, their values are still higher than for fresh sample, denoting that the solid is consuming less reducing species per unit of time. As aforementioned, this phenomenon can be attributed to sintering of the solid. Despite of the increment in the amount of reducible mass after combustions, the influence of thermal degradation of the solid keeps lowering the rate at which the oxygen carrier is reduced. On the other hand, there does not seem to be a clear decrease in the time needed to reduce the solid between cycles: all of them achieve a stable value of CO ratio of 0.9 after ca. 28 min. Note that the steady value of CO ratio, only depends on thermodynamic equilibria between solid and gaseous species at a given temperature, and that this is the same regardless of the nature of the solid, being predictable by minimization of the Gibbs free energy (ΔG).

Analyzing the reduction stages of iron ore (Figure 6b), the addition of coke combustion stages causes a steep decrease of the CO ratio along the period in which the solid is reduced, in comparison with that of solid before combustion stages (i.e. 4^{th} reduction in Fig 6b). After

combustion stages, subsequent reductions present similar CO ratio curves than the one for fresh solid. More in detail, higher decreases in the CO ratio along the period in which the solid is reduced from Fe_2O_3 to Fe_3O_4 (see Figure 2a, period A_1) were obtained after combustions, being able to be associated with a higher content in hematite at those circumstances.

Regarding the differences between both solids based in hematite, the evolution of the CO ratio shown in Figure 6a and Figure 6b is analogous to that previously analyzed in an earlier work of this research group [12]. The most significant difference between them occurs along the first reduction (fresh solid), where iron ore presents higher values of the CO ratio in the period in which reduction of hematite to magnetite takes place (period A_1, Figure 2a). Its lower amount of accessible iron oxide and moderate rate of reduction, probably due to the impurities present in this solid, causes a smaller consumption of reducing agents along this period. On the contrary, in the period linked with the transformation of magnetite in iron (period A_2, Figure 2a), situation reverts, being greater the rate of reduction of *triple* oxide than that of iron ore. In any case, after applying the coke combustion stages, the evolution of the CO ratio, as well as the amount of H_2 produced in the subsequent oxidation stage with steam (showed in Figure 5), become similar.

In case of *cobalt ferrite*, after the introduction of the combustion steps, the time required to completely reduce the solid (Figure 6c) is like that of the starting material. Nevertheless, the values of CO ratio at early times is lower than for the fresh solid, denoting that the reduction is more vigorous in material that have suffered interspersed combustion. The conclusion is that the course of redox cycles has caused an oxide with better redox properties than the starting material, being attributed, again, to the segregation of species. The behaviour of this solid is qualitatively different than that shown by the other two oxides: the production of hydrogen is much more stable along the redox cycles (Figure 5) obtaining similar productions to those of the other oxygen carriers tested.

3.4 Influence of the kind of bed pretreatment in the iron ore activity

Two additional tests were carried out to determine possible causes of the substantial raise in hydrogen production observed for iron ore. Figure 7 shows the results of H_2 production (g) per 100 g of solid, compared with the first 5 cycles of the iron ore regular operation (R.O.) tests (i.e. 4 cycles of reduction + reoxidation with steam and then a stage of oxidation with diluted oxygen) shown in Figure 5. The first test, tagged as Pret.A, consisted in subjecting the fresh iron ore bed to a simulated coke combustion stage employing the same conditions as in previous tests (i.e. oxidation with diluted oxygen). The second test (Pret.B), was performed carrying out a reduction step and substituting the subsequent regular reoxidation with steam, by a direct combustion with diluted oxygen (see details in the experimental section). Results shows that Pret.A treatment does not provoke any significant increase of the hydrogen production. On the contrary, the second one (Pret.B), causes a substantial upraise of around 70% (average value) in the mass of hydrogen produced by cycle, compared to those obtained using the regular operation method. It is important noting that these differences were cancelled in the fifth cycle, showing results comparable to those obtained in absence of any pretreatment (i.e. regular operation). Based in the behavior observed, it could be formulated as hypothesis that the hot spots generated as consequence of the combustion of the coke accumulated in the bed, would cause a rearrangement of the crystal structure of the ore that triggers the activation of portions of Fe_2O_3 that otherwise remained inert. This gain in activity has been observed with this same ore by other researchers in other redox applications such as chemical looping combustion (CLC) [39], as well as with iron ores with different composition [40]. The application of Pret.B treatment, has allowed a production of hydrogen like that obtained with *triple* oxide.

4. CONCLUSIONS

In the present work it has been analyzed the influence of interspersing combustion stages with diluted oxygen between every four reduction-oxidation cycles of steam in the so-called *steam-iron process* (SIP), in order to remove the eventual carbonaceous deposits generated along reduction stages. This strategy not only avoids reactor clogging by coke, but increases the amount of accessible oxide, increasing the mass of hydrogen that can be released in oxidations with steam. The study has been performed with three different oxygen carriers: two synthetic oxides (*triple* oxide and cobalt ferrite) and a natural oxide (iron ore). For oxides based in hematite (iron ore, and *triple* oxide), it has been verified that the introduction of coke combustion stages breaks down the trend to sintering, allowing to extend the useful life of the solid. In tests with iron ore, the introduction of combustion stages causes a significant activation of the material, allowing to obtain similar yields to those obtained with *triple* oxide. In addition, if iron ore is subjected to a first cycle of reduction and subsequent combustion of the accumulated coke, it is possible to raise the hydrogen production along the first redox cycles.

The excellent behavior of the iron ore supposes an interesting cheaper alternative versus synthetic (*triple*) oxide. On the other side, application of SIP supposes an added value alternative for this material: once exhausted it could be still being used in its traditional industrial applications as raw material for pigments, dyes, etc.

Use of cobalt ferrite allows the production of a much more stable hydrogen flow due to its greater resistance to sintering. The segregation of part of the ferrite upon cycles, to other simpler constituent oxides (Co_3O_4 and Fe_3O_4) instead of the original cobalt ferrite, might explain the increase in activity observed empirically. On the other hand, this phenomenon might be envisaged as a disadvantage in applications in which the redox reactions must be carried out at high temperatures, since this behavior causes a severe weakening of the structure, increasing the sintering of the solid [34].

Regardless of the solid used, the introduction of interspersed combustion stages with diluted oxygen allowed uninterrupted production of high purity hydrogen ($CO_x \leq 50$ ppm) over 13

redox cycles achieving similar averaged yields of H_2 per 100 g of solid between the three oxygen carriers tested.

5. ACKNOWLEDGEMENTS

Financial support for this work has been provided by the Spanish *Ministerio de Economía y Competitividad* (MINECO), through project ENE2013-44350-R and CTQ2016-77277-R. J. Lachén also thanks the same institution for the grant BES-2014-067984. Financial aid for the maintenance of the consolidated research group *CREG* has been provided by the *Fondo Social Europeo* (FSE) through *Gobierno de Aragón* (Aragón, Spain).

REFERENCES

[1] Moliner R, Lázaro MJ, Suelves I. Analysis of the strategies for bridging the gap towards the Hydrogen Economy. Int J Hydrogen Energy 2016;41:19500–8. doi:10.1016/j.ijhydene.2016.06.202.

[2] Nejat Veziroğlu T. Quarter century of hydrogen movement 1974–2000. Int J Hydrogen Energy 2000;25:1143–50. doi:10.1016/S0360-3199(00)00038-0.

[3] Muradov N. Low to near-zero CO2 production of hydrogen from fossil fuels: Status and perspectives. Int J Hydrogen Energy 2017;42:14058–88. doi:10.1016/j.ijhydene.2017.04.101.

[4] Porter RTJ, Fairweather M, Kolster C, Mac Dowell N, Shah N, Woolley RM. Cost and performance of some carbon capture technology options for producing different quality CO2 product streams. Int J Greenh Gas Control 2017;57:185–95. doi:10.1016/j.ijggc.2016.11.020.

[5] Messerschmitt A. Process of producing hydrogen.- U.S. Patent No. 971,206. 971, 206, 1910.

[6] Luo M, Yi Y, Wang S, Wang Z, Du M, Pan J, et al. Review of hydrogen production using chemical-looping technology. Renew Sustain Energy Rev 2018;81:3186–214. doi:10.1016/j.rser.2017.07.007.

[7] Mendiara T, García-Labiano F, Abad A, Gayán P, de Diego LF, Izquierdo MT, et al. Negative CO2 emissions through the use of biofuels in chemical looping technology: A review. Appl Energy 2018;232:657–84. doi:10.1016/J.APENERGY.2018.09.201.

[8] Voitic G, Hacker V. Recent advancements in chemical looping water splitting for the production of hydrogen. RSC Adv 2016;6:98267–96. doi:10.1039/C6RA21180A.

[9] Plou J, Durán P, Herguido J, Peña JA. Hydrogen from synthetic biogas by catalyzed

MDR and SIP: Screening of catalyst and iron oxide mixtures. Fuel 2015;140:470–6. doi:10.1016/j.fuel.2014.09.116.

[10] Nestl S, Voitic G, Lammer M, Marius B, Wagner J, Hacker V. The production of pure pressurised hydrogen by the reformer-steam iron process in a fixed bed reactor system. J Power Sources 2015;280:57–65. doi:10.1016/j.jpowsour.2015.01.052.

[11] Lorente E, Peña JA, Herguido J. Cycle behaviour of iron ores in the steam-iron process. Int J Hydrogen Energy 2011;36:7043–50. doi:10.1016/j.ijhydene.2011.03.069.

[12] Lachén J, Plou J, Durán P, Herguido J, Peña JA. Iron oxide ores as carriers for the production of high purity hydrogen from biogas by steam–iron process. Int J Hydrogen Energy 2017;42:13607–16. doi:10.1016/j.ijhydene.2016.11.152.

[13] Bleeker MF, Veringa HJ, Kersten SRA. Deactivation of iron oxide used in the steam-iron process to produce hydrogen. Appl Catal A Gen 2009;357:5–17. doi:10.1016/j.apcata.2008.12.032.

[14] Hui W, Takenaka S, Otsuka K. Hydrogen storage properties of modified fumed-Fe-dust generated from a revolving furnace at a steel industry. Int J Hydrogen Energy 2006;31:1732–46. doi:10.1016/j.ijhydene.2005.12.010.

[15] Haider SK, Azimi G, Duan L, Anthony EJ, Patchigolla K, Oakey JE, et al. Enhancing properties of iron and manganese ores as oxygen carriers for chemical looping processes by dry impregnation. Appl Energy 2016;163:41–50. doi:10.1016/j.apenergy.2015.10.142.

[16] Ettabirou M, Dupré B, Gleitzer C. Nucleation and early growth of magnetite on synthetic and natural hematite crystals. React Solids 1986;1:329–43. doi:10.1016/0168-7336(86)80025-0.

[17] Bleeker MF, Veringa HJ, Kersten SRA. Pure Hydrogen Production from Pyrolysis Oil Using the Steam Iron Process: Effects of Temperature and Iron Oxide Conversion in the

Reduction. Ind Eng Chem Res 2010;49:53–64.

[18] Cocchi S, Mari M, Cavani F, Millet JMM. Chemical and physical behavior of CoFe2O4 in steam-iron process with methanol. Appl Catal B-Environmental 2014;152:250–61. doi:10.1016/j.apcatb.2014.01.040.

[19] Campo R, Durán P, Plou J, Herguido J, Peña JA. Combined production and purification of hydrogen from methanol using steam iron process in fixed bed reactor. J Power Sources 2013;242:520–6. doi:10.1016/j.jpowsour.2013.05.146.

[20] Hormilleja E, Durán P, Plou J, Herguido J, Peña JA. Hydrogen from ethanol by steam iron process in fixed bed reactor. Int J Hydrogen Energy 2014;39:5267–73. doi:10.1016/j.ijhydene.2014.01.002.

[21] Plou J, Lachén J, Durán P, Herguido J, Peña JA. Pure hydrogen from lighter fractions of bio-oil by steam-iron process: Effect of composition of bio-oil, temperature and number of cycles. Fuel 2017;203:452–9. doi:10.1016/j.fuel.2017.04.127.

[22] Deublein D, Steinhauser A. Biogas from waste and renewable resources. An introduction. Wiley VCH; 2008.

[23] Hagos K, Zong J, Li D, Liu C, Lu X. Anaerobic co-digestion process for biogas production: Progress, challenges and perspectives. Renew Sustain Energy Rev 2017;76:1485–96. doi:10.1016/j.rser.2016.11.184.

[24] Kadam R, Panwar NL. Recent advancement in biogas enrichment and its applications. Renew Sustain Energy Rev 2017;73:892–903. doi:10.1016/J.RSER.2017.01.167.

[25] Leonzio G. Upgrading of biogas to bio-methane with chemical absorption process: simulation and environmental impact. J Clean Prod 2016;131:364–75. doi:10.1016/j.jclepro.2016.05.020.

[26] Herrer M, Plou J, Durán P, Herguido J, Peña JA. Hydrogen from synthetic biogas via

SIP using NiAl2O4 catalyst: Reduction stage. Int J Hydrogen Energy 2015;40:5244–50. doi:10.1016/j.ijhydene.2015.01.063.

[27] Plou J, Duran P, Herguido J, Pena JA. Purified hydrogen from synthetic biogas by joint methane dry reforming and steam-iron process: Behaviour of metallic oxides and coke formation. Fuel 2014;118:100–6. doi:10.1016/j.fuel.2013.10.069.

[28] Lachén J, Durán P, Peña JA, Herguido J. High purity hydrogen from coupled dry reforming and steam iron process with cobalt ferrites as oxygen carrier: Process improvement with the addition of NiAl2O4 catalyst. Catal Today 2017;296:163–9. doi:10.1016/j.cattod.2017.04.046.

[29] Kirchnerova J, Alifanti M, Delmon B. Evidence of phase cooperation in the LaCoO3-CeO2-Co3O4 catalytic system in relation to activity in methane combustion. Appl Catal A Gen 2002;231:65–80. doi:10.1016/S0926-860X(01)00903-6.

[30] Lázaro MJ, Echegoyen Y, Alegre C, Suelves I, Moliner R, Palacios JM. TiO2 as textural promoter on high loaded Ni catalysts for methane decomposition. Int J Hydrogen Energy 2008;33:3320–9. doi:10.1016/j.ijhydene.2008.03.050.

[31] Al-Ubaid A, Wolf EE. Steam reforming of methane on reduced non-stoichiometric nickel aluminate catalysts. Appl Catal 1988;40:73–85. doi:10.1016/S0166-9834(00)80427-3.

[32] Peña JA, Lorente E, Romero E, Herguido J. Kinetic study of the redox process for storing hydrogen. Catal Today 2006;116:439–44. doi:10.1016/j.cattod.2006.05.068.

[33] Lachén J, Herguido J, Peña JA. Production and purification of hydrogen by biogas combined reforming and steam-iron process. Int J Hydrogen Energy 2018. doi:10.1016/j.ijhydene.2018.04.151.

[34] Orfila M, Linares M, Molina R, Botas JÁ, Sanz R, Marugán J. Perovskite materials for hydrogen production by thermochemical water splitting. Int J Hydrogen Energy

2016;41:19329–38. doi:10.1016/j.ijhydene.2016.07.041.

[35] Klissurski DG, Uzunova EL. Cation-deficient nano-dimensional particle size cobalt–manganese spinel mixed oxides. Appl Surf Sci 2003;214:370–4. doi:10.1016/S0169-4332(03)00524-5.

[36] Aston VJ, Evanko BW, Weimer AW. Investigation of novel mixed metal ferrites for pure H2 and CO2 production using chemical looping. Int J Hydrogen Energy 2013;38:9085–96. doi:10.1016/j.ijhydene.2013.05.078.

[37] Li Y, Li D, Wang G. Methane decomposition to COx-free hydrogen and nano-carbon material on group 8-10 base metal catalysts: A review. Catal Today 2011;162:1–48. doi:10.1016/j.cattod.2010.12.042.

[38] Zhu M, Song Y, Chen S, Li M, Zhang L, Xiang W. Chemical looping dry reforming of methane with hydrogen generation on Fe2O3/Al2O3 oxygen carrier. Chem Eng J 2019;368:812–23. doi:10.1016/J.CEJ.2019.02.197.

[39] Mendiara T, Pérez R, Abad A, de Diego LF, García-Labiano F, Gayán P, et al. Low-Cost Fe-Based Oxygen Carrier Materials for the i G-CLC Process with Coal. 1. Ind Eng Chem Res 2012;51:16216–29. doi:10.1021/ie302157y.

[40] Adánez J, Cuadrat A, Abad A, Gayán P, de Diego LF, García-Labiano F. Ilmenite activation during consecutive redox cycles in chemical-looping combustion. Energy and Fuels 2010;24:1402–13. doi:10.1021/ef900856d.

FIGURE CAPTIONS

Figure 1.- Conceptual diagram of (a) Steam-Iron redox cycle (alternating reductions and oxidations) and (b) timeline alternating redox cycles and interspersed coke combustions with diluted oxygen.

Figure 2.- Molar flows of species in the exhaust gases during the first reduction stage at 700 ºC for different oxygen carriers tested: (a) iron ore and *triple* oxide; (b) cobalt ferrite.

Figure 3.- CO ratio (eq. 1) along four consecutive reduction stages at 700 ºC using (a) iron ore, (b) *triple* oxide and (c) cobalt ferrite as oxygen carrier.

Figure 4.- Mass of hydrogen (g) obtained in reoxidations with steam per 100 g of solid along the first four redox cycles.

Figure 5.- Mass of hydrogen (g) obtained in oxidations per 100 g of solid along 13 redox cycles using interspersed coke combustion stages every 4 redox cycles.

Figure 6.- CO ratio at the exit of the reactor along reduction stages following coke combustion stages using (a) iron ore (b) *triple* oxide and c) cobalt ferrite as oxygen carriers. CO ratio along first and fourth reductions are shown as comparison criterium.

Figure 7.- Mass of hydrogen (g) per 100 g of iron ore produced along redox cycles applying different pretreatments: *i) Regular Operation* (R.O.) consisting in five consecutive redox cycles and coke combustion with diluted oxygen after 4^{th} cycle. *ii) Pretreatment A* (Pret. A) subjecting fresh iron ore to a combustion stage prior to regular operation (R.O.). iii) *Pretreatment B* (Pret.B) consisting of reduction followed by coke combustion and regular operation.

Figure 1

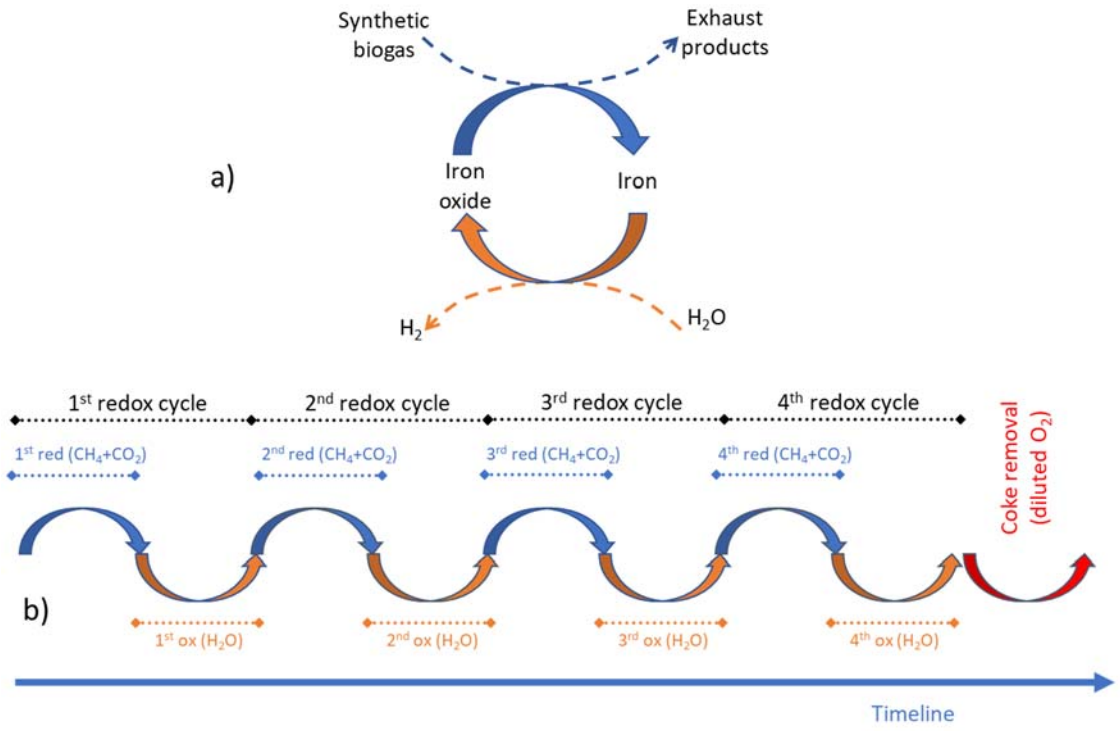
Synthetic biogas
Exhaust products
a)
Iron oxide
Iron
H_2
H_2O
1st redox cycle
2nd redox cycle
3rd redox cycle
4th redox cycle
1st red (CH_4+CO_2)
2nd red (CH_4+CO_2)
3rd red (CH_4+CO_2)
4th red (CH_4+CO_2)
Coke removal (diluted O_2)
b)
1st ox (H_2O)
2nd ox (H_2O)
3rd ox (H_2O)
4th ox (H_2O)
Timeline

Figure 2

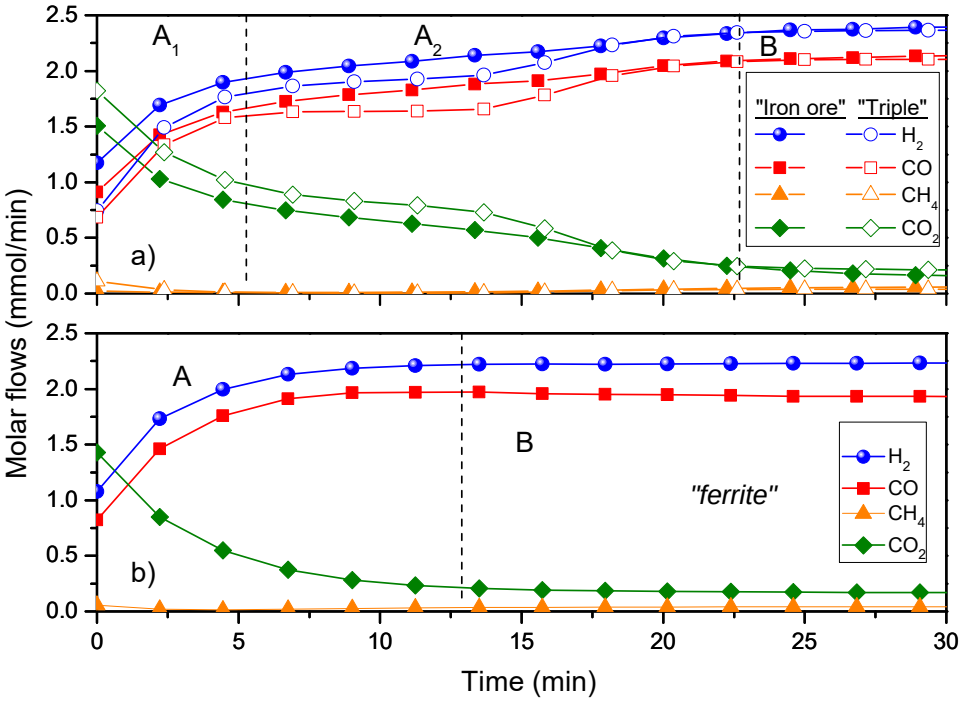
A1
A2
B
"Iron ore"
"Triple"
H2
CO
CH4
CO2
a)
A
B
"ferrite"
b)
Molar flows (mmol/min)
Time (min)
0.0
0.5
1.0
1.5
2.0
2.5
0
5
10
15
20
25
30

Figure 3

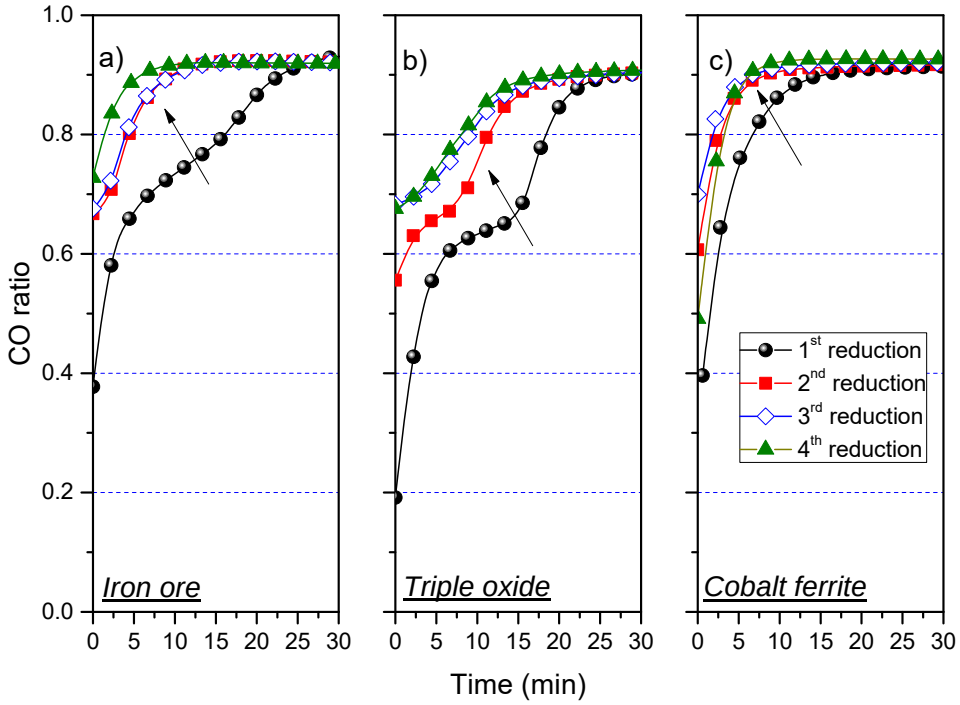
a)
b)
c)
CO ratio
Time (min)
Iron ore
Triple oxide
Cobalt ferrite
1st reduction
2nd reduction
3rd reduction
4th reduction

Figure 4

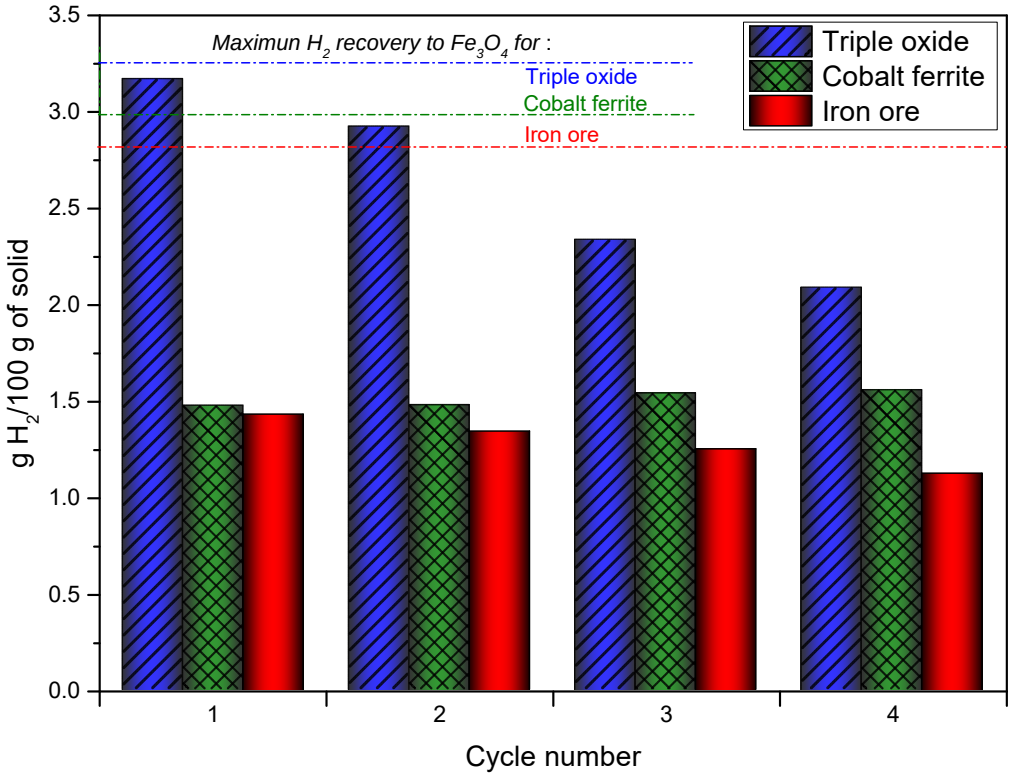
Maximun H_2 recovery to Fe_3O_4 for :
Triple oxide
Cobalt ferrite
Iron ore
Triple oxide
Cobalt ferrite
Iron ore
g H_2/100 g of solid
0.0
0.5
1.0
1.5
2.0
2.5
3.0
3.5
1
2
3
4
Cycle number

Figure 5

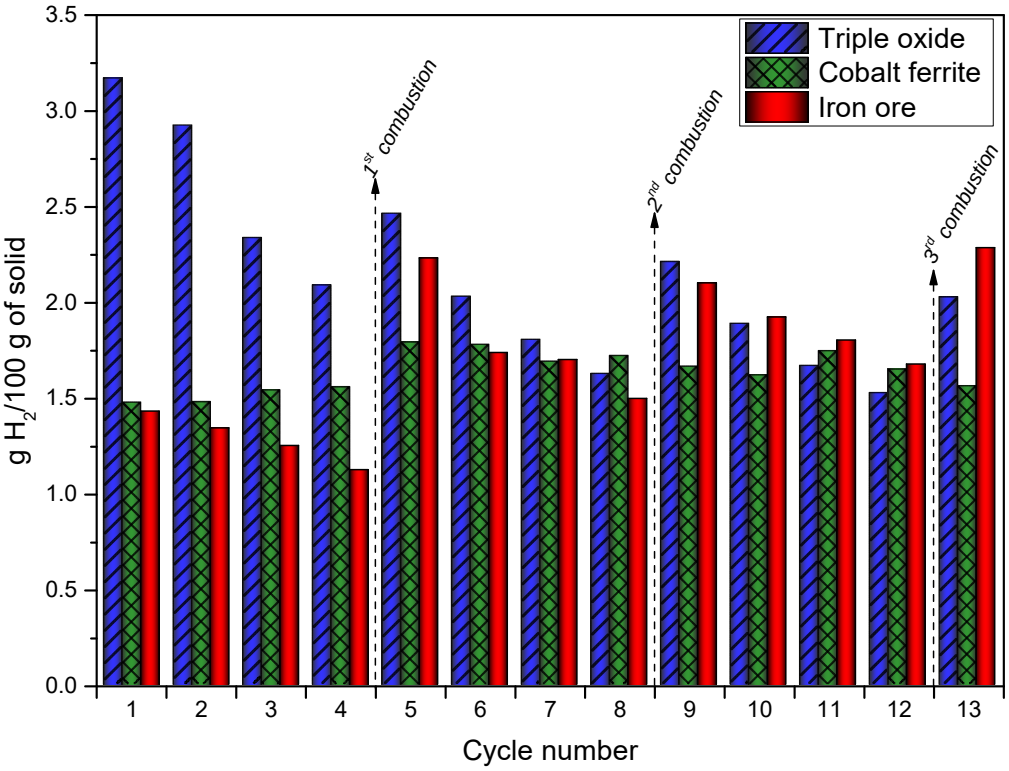
Triple oxide
Cobalt ferrite
Iron ore
1st combustion
2nd combustion
3rd combustion
g H2/100 g of solid
Cycle number
0.0
0.5
1.0
1.5
2.0
2.5
3.0
3.5
1
2
3
4
5
6
7
8
9
10
11
12
13

Figure 6

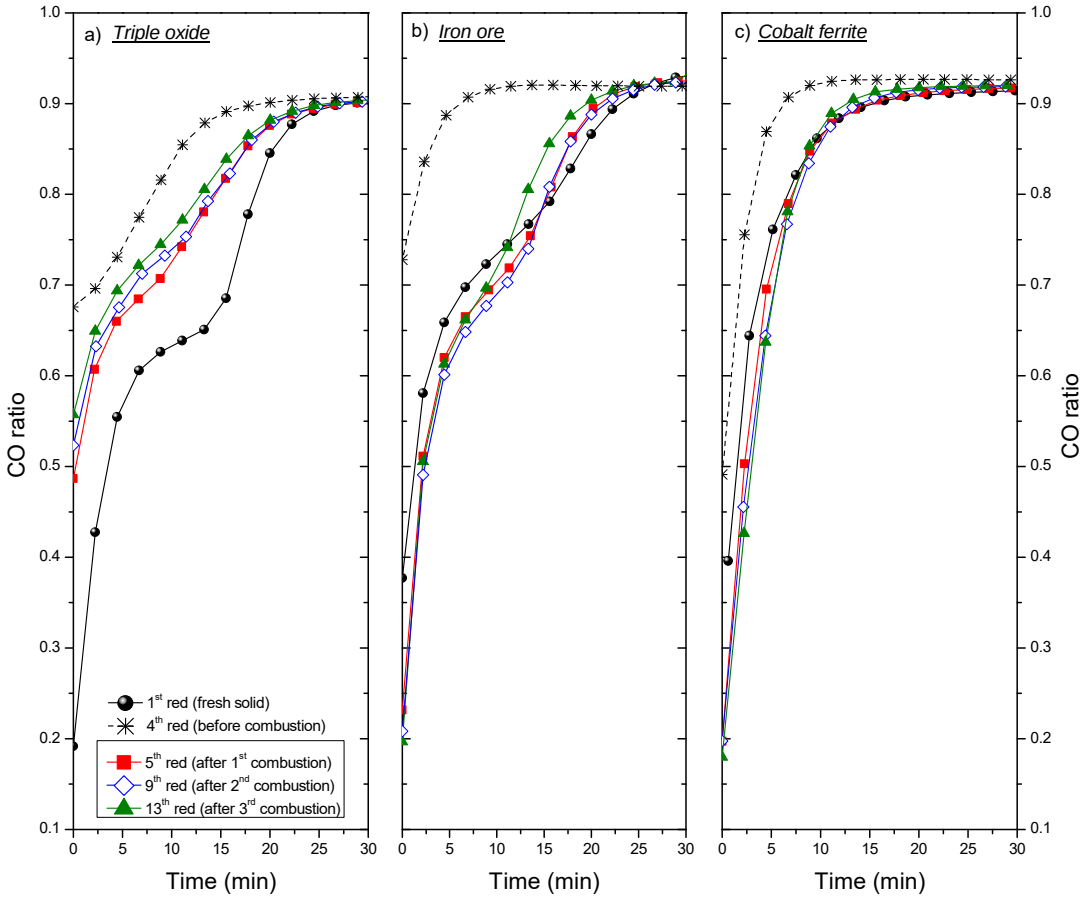
a) Triple oxide
b) Iron ore
c) Cobalt ferrite
CO ratio
Time (min)
1st red (fresh solid)
4th red (before combustion)
5th red (after 1st combustion)
9th red (after 2nd combustion)
13th red (after 3rd combustion)

Figure 7

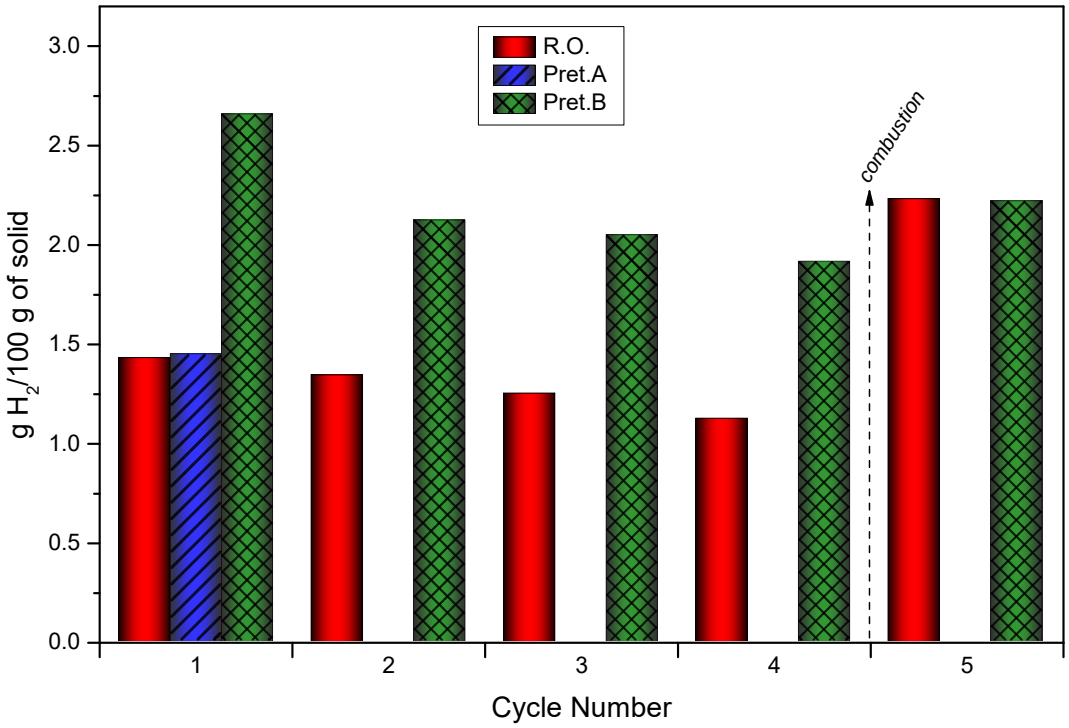
R.O.
Pret.A
Pret.B
combustion
g H2/100 g of solid
3.0
2.5
2.0
1.5
1.0
0.5
0.0
1
2
3
4
5
Cycle Number

J. Lachén, J. Herguido and J.A. Peña*

High purity hydrogen from biogas via Steam Iron Process: preventing reactor clogging by interspersed coke combustions

Highlights

- *Hydrogen produced by catalytic dry reforming of methane and carbon dioxide*
- *Reaction products (H_2 and CO) reduce iron oxides present in the bed*
- *Small amounts of coke produced along reductions accumulate along consecutive cycles*
- *Analysis of the effect of interspersing coke combustion stages after 4 redox cycles*
- *Reoxidation with steam release high purity hydrogen if operated al low temperature*